DOI: 10.21062/mft.2024.085 http://www.journalmt.com

Quantification and Verification of Swingarm Structural Characteristics Through Numerical Simulation and Photogrammetry

Lukas Gregor (0000-0002-3364-4510), Jan Zouhar (0000-0001-8031-8366), Radim Kupcak (0009-0003-6630-236X)
Department of Machining Technology, Institute of Manufacturing Technology, Faculty of Mechanical Engineering, Brno University of Technology, Technicka 2896/2, Brno 616 69, Czech Republic.
E-mail: Lukas.Gregor1@vutbr.cz, zouhar@fme.vutbr.cz, 170299@vutbr.cz

Composite materials have consistently been applied in areas where a combination of properties such as strength, stiffness, and low weight is crucial. Motorcycle construction is no exception, as these parameters significantly impact riding characteristics, safety, and overall performance. This article focuses on quantifying the torsional and vertical stiffness of a single-sided swingarm made of carbon fiber reinforced polymer (CFRP) using finite element analysis (FEA) and verifying these results through experimental measurements. To enhance the accuracy of the simulations, which involve complex geometries and anisotropic materials, the material properties of selected fabrics used in the prototype production were measured. Specific fixtures were designed for the experimental measurements, enabling the application of torsional moments and vertical forces. Deformation under these loads was evaluated using the TRITOP photogrammetric system, which tracks deformations by monitoring the displacement of reference points under static load conditions and comparing them to a reference, unloaded state. Based on the acquired data, the overall stiffness values and their distribution along the length of the swingarm were calculated. The results showed a significant difference between simulation and reality. For the overall torsional stiffness, the simulated value was 249 N·m/°, while the measured was 270 N·m/°, showing a discrepancy of 7.7%. The vertical stiffness value from simulation was 414 N/mm, compared to 411 N/mm from experimental measurements, with a minimal difference of -0.7%. The stiffness distribution along the length of the swingarm exhibited a correlation, but with notable variation in certain areas. This confirms that accurately simulating CFRP parts with complex geometries is highly challenging, partly due to the sensitivity of the manufacturing process. Therefore, verification through experimental measurement is considered good practice.

Keywords: Swingarm, Torsional stiffness, CFRP, Photogrammetry, Stiffness distribution

1 Introduction

The dynamics of motorcycles, characterized by their movement in three dimensions, significantly differ from the dynamics of automobiles. This distinction results in a high degree of instability, and the primary task for designers and engineers is to minimize these negative impacts on motorcycle control under normal operational conditions [1]. The fundamental modes of instability during riding were discussed by Sharp in 1971 [2]. They include capsize, a non-oscillatory motion where the motorcycle tends to fall to one side at low speeds, weave, an oscillatory side-to-side motion of the entire motorcycle with a frequency of 0.2 to 3.4 Hz, and wobble, a rotational oscillation of the front fork relative to the motorcycle frame at a frequency of 9 Hz. In addition to these modes, several other instability modes have been defined and confirmed by Cossalter et al. [3], though they are not relevant to the context of this study.

The long-term growth in the computational power of modern computers has enabled the use of efficient tools such as multibody simulations [4], which allow for the prediction of these modes, vehicle properties and parameter optimization before the prototype production. This leads to cost reduction and accelerates the development process [5]. However, each simulation is only an approximation of reality, and its final accuracy depends on the precision of the individual inputs. For motorcycles, some of these inputs are the structural properties of the swingarm. These properties can be obtained through FEA, but they can be relatively inaccurate when dealing with CFRP composites of complex geometry [6]. Therefore, this work focuses on verifying the numerical simulation of a CFRP swingarm using photogrammetric measurements of structural properties and their respektive distributions.

1.1 Impact of structural components

When focusing on structural components of motorcycles such as the frame and the swingarm, literature indicates that they have a significant impact on

the resulting dynamics and the aforementioned instability modes. The influence of frame stiffness on these modes is extensively described, and a summary was provided by Lake et al. [1]. Frame stiffness increases wobble speed and weave speed, wobble is much more sensitive than weave to stiffness, and torsional stiffness impacts wobble more than lateral stiffness [7–14].

The impact of the structural properties of the swingarm is different and not as thoroughly explored. Cossalter et al. [15] confirmed that stiffness of the swingarm has only a minor influence on capsize and wobble modes but affects the damping of the weave mode at medium and high speeds. Unlike other authors, they also distinguish between the effects of torsional and lateral stiffness. Lateral stiffness slightly destabilizes the weave mode at very high speeds, while torsional stiffness has the opposite effect, stabilizing it. This assertion is confirmed by Lot et al. [16], who additionally note that increasing torsional stiffness raises the weave frequency and the weave damping [10, 17].

Lateral flexibility is also important because it allows partial springing at large lean angles of the motorcycle when the conventional suspension system ceases to function [18].

The authors do not address vertical stiffness, as the suspension unit operates in this plane. However, it is generally recommended that the vertical stiffness should be at least five times the stiffness of the rear suspension spring to ensure the proper functioning of the suspension system [19, 20]. All mentioned structural stiffnesses are shown in Fig. 1 and Tab. 1 provides an overview of the swingarm structural properties based on the literature review.

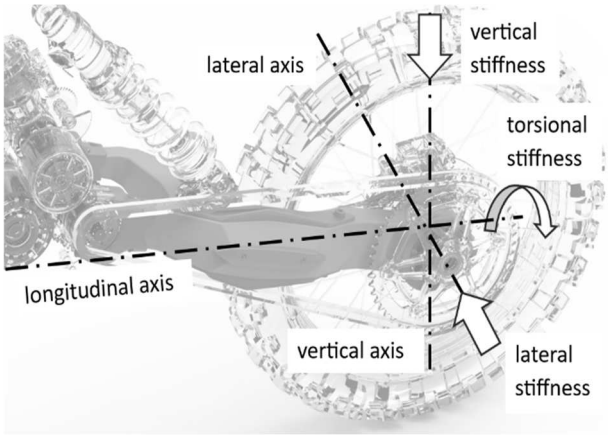

Fig. 1 *Swingarm structural stiffnesses*

Tab. 1 *Literature review of swingarm structural properties*

Resource	Torsional stiffness [N·m/°]	Lateral stiffness [N/mm]	Vertical stiffness [N/mm]
Limebeer and Sharp [17]	210	x	x
Cossalter [5]	1000-2000	800 - 1600	x
Taraborelli [21]	1350	1760	1083
Taraborelli [21]	960	640	623
Armentani [22]	103	x	x
Armentani [22]	140	x	x
Armentani [22]	140	x	x
Smith[19]	550	x	500
Risitano [23]	670	x	x
Risitano [23]	890	x	x
Risitano [23]	1330	x	x

1.2 Advances and challenges in the use of CFRP

Manufacturers began experimenting with carbon fiber composite materials in motorcycles as early as the 1990s. However, the benefits of this application were not significant enough to substitute structural components, as seen in Formula 1 [24, 25]. For motorcycles, the use of carbon fiber composites was long restricted to "covering and visual" elements rather than structural components. One reason for this was the internal combustion motorcycle's construction, where the engine itself bore much of the load, rendering the benefits of composite parts less substantial. Today, the situation is changing with the advent of electric motorcycles, presenting several opportunities for the use of carbon composites. This shift aims to minimize weight due to the low specific energy density of battery cells and the resulting high weight [26–28]. Moreover, the different design of the electric power unit allows a completely different conception of structural elements, as seen in motorcycles like Novus or Samurai [29, 30] The increasing trend in the use of composite materials across nearly all industries further confirms their relevance [31–35].

Attempts to apply composite materials to the swingarm date back to 1982 [36]. Initially, these attempts focused on material substitution, which did not fully exploit the potential of these materials. More interestingly, Smith's work [19] combined numerical and experimental measurements of the swingarm properties. He demonstrated that, compared to the original aluminum swingarm, a 29% weight reduction was possible using composite materials. However, he

did not compare the structural properties to the original swingarm, relying instead on literature reviews. One notable finding was the significant variation in results between numerical simulations and experimental measurements, with discrepancies of 4% for vertical stiffness and 28% for torsional stiffness. Smith attributed these differences to the complicated geometry of the part, which makes it impossible to model overlaps.

The inaccuracy of simulations for complex composite parts, as seen in Smith's article, is a well-documented issue, as demonstrated by Hosein and Grafinder's study [37]. The authors compared theoretical calculations with several variants of numerical simulations on relatively simple geometries, revealing significant differences. The study highlights the strengths of FEA for specific composite applications while pointing out potential pitfalls from incorrect approaches, methods, or the inherent challenges of composite simulations.

A study by Airoldi et al. [38] also explores the application of composite materials to replace the current swingarm design. The author employs multi-objective optimization of the composite layup to tune the swingarm's parameters according to defined permissible deformation ranges for vertical and longitudinal stiffness while minimizing weight and twist angle. This study indicates that technological modifications to the existing aluminum design, coupled with multi-objective simulations, could maintain torsional stiffness while reducing the swingarm's weight by almost 10%. However, considering Smith's findings [19], the reality may differ.

Significant benefit of using CFRP composites is their resistance to fatigue compared to aluminum alloys. This increased fatigue resistance can lead to longer-lasting components and potentially lower maintenance requirements over the lifespan of the motorcycle [39–41]. Structural components could also benefit from usage of fibre-hybrid composites, where the addition of aramid or flax fiber can bring specific properties such as damping or could hold the fragments of part together in case of crash [33, 41].

In summary, polymer composites are modern materials suitable for constructing structural components, especially due to their specific stiffness-to-weight and strength-to-weight ratios. Another benefit is their anisotropic properties, allowing for the maximal exploitation of the material's potential and engineering design for specific applications using modern tools like FEA combined with multi-objective optimizations. However, their complexity and sensitivity to the manufacturing process, quality, design, and material used are significant disadvantages [42–46].

2 Design and optimization of the swingarm structure

The strength and safety of the swingarm construction are crucial from a structural integrity standpoint. Based on input parameters from the CAD model, including motorcycle kinematics, center of gravity position, maximum weight of the motorcycle with the rider, weight distribution, peak safety up to 5g, and other parameters, worst-case riding scenarios were defined using a ½ dynamic model of the motorcycle with two degrees of freedom. These scenarios include braking, jumping, and cornering. The force vectors are listed in Tab. 2, and the points of force application are shown in Fig. 2.

Tab. 2 *Worst case scenarios*

Loading condition	Point of force	F_X [N]	F_Y [N]	F_Z [N]
Braking	Centre of gravity	2942	0	-2452
Jump	Rear suspension	-11126	0	-16620
Jump	Seat and footpegs	0	0	-1000
Cornering	Contact point at rear wheel and road surface	0	-251	938

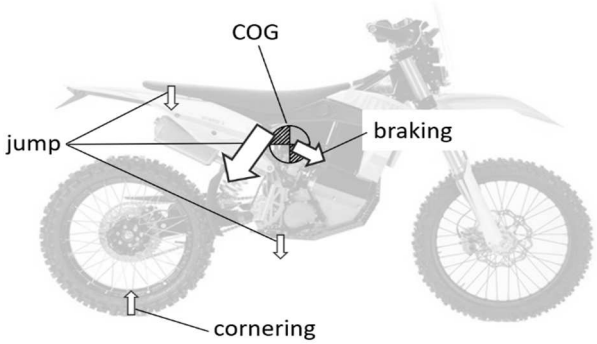

Fig. 2 *Worst case scenarios – acting forces*

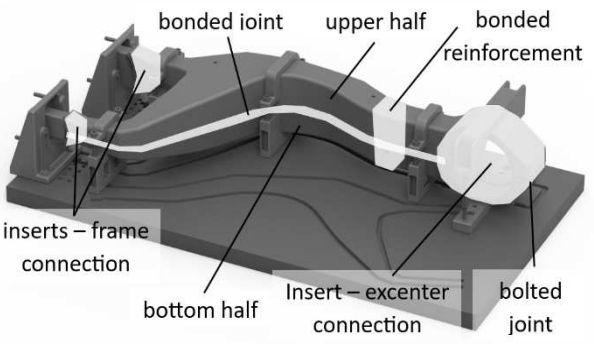

Fig. 3 *Swingarm design*

The construction of the swingarm is illustrated in Fig. 3. It consists of two nearly symmetrical CFRP parts precisely joined together with structural epoxy adhesive. The assembly includes bonded aluminum and CFRP inserts that ensure the transfer of forces beyond local areas and provide connections to other parts of the motorcycle, such as the frame, suspension, eccentric, or brake.

To optimize the design, the following objectives were established based on a literature review and the defined worst-case scenarios. Considering that excessive increases in parameters such as stiffness lead to increased weight, recommended ranges are provided. Exceeding these ranges does not result in significant benefits and instead increases unsprung mass.

- Maximize torsional stiffness (recommended range 1000 – 2000 N·m/°),
- Maximaze vertical stiffness (recommended range 500 – 1500 N/mm, at least 5 times the spring stiffness),
- Reduce lateral stiffness (recommended range 800 – 1600 N/mm),
- Minimize weight,
- Ensure sufficient strength and safety (worst case scenarios, Tab. 2).

For the prototype production, high strength (HS) carbon fiber T700G by Toray and an epoxy resin DT120 by Deltapreg were selected. To enhance aesthetic value, a twill weave fabric with a surface density of 630 g/m² was chosen for the visible side. Additionally, biaxial reinforcements (±45° orientation) with the same fiber and a surface density of 300 g/m² were used to improve mechanical properties. During production, debulking was performed after the 1st and 4th layers to ensure better adherence and material consolidation.

The chosen manufacturing technology is the prepreg method utilizing an autoclave. The primary reasons for this choice are precision and repeatability, achieved through prepared cut patterns on a cutting plotter. The use of an autoclave ensures good material consolidation without unnecessary defects [47].

For this study, a simple symmetrical preliminary layup ($0°_T/0°_B/45°_B/0°_B/45°_B/0°_B/0°_T$) with a total thickness of 2.7 mm was created to verify the concept and chosen manufacturing technology (Tab. 3). This initial layup does not include local reinforcements and is not expected to meet all required structural properties. It essentially follows a trial-and-error approach, with the prototype being made before FEA were conducted. Based on the insights gained from this study, a new layup will be developed using multi-objective optimization.

Tab. 3 *Swingarm preliminary layup*

Stacking sequence	Fabric	Fiber orientation	Style	weight [g/m²]	thickness [mm]
1	HS Carbon	0°/90°	Twill 2/2	630	0.6
		debulk			
2	HS Carbon	+45°/-45°	Biax	300	0.3
3	HS Carbon	0°/90°	Biax	300	0.3
4	HS Carbon	+45°/-45°	Biax	300	0.3
		debulk			
5	HS Carbon	0°/90°	Biax	300	0.3
6	HS Carbon	+45°/-45°	Biax	300	0.3
7	HS Carbon	0°/90°	Twill 2/2	630	0.6

3 Experimental measuring

The measurement of the structural properties of the swingarm was conducted statically using calibrated weights and took place before the FEA itself. Deformations due to the applied load were recorded with the TRITOP photogrammetric measurement device, which accurately captures the positions of prepared reference points in 3D space. The principle involves capturing the points in a reference (unloaded) state and then capturing the same points under load. It is essential to place reference points on a rigid body that does not deform or change position during the measurement process, serving to compensate for motion in individual measurements. This method effectively records not only the overall stiffness but also the stiffness distribution along the length of the swingarm. [48, 49]

The accuracy of the measurements was verified using two calibration rods, demonstrating a measurement accuracy with a maximum deviation of 0.02 mm/m. Five measurements with different weights were conducted for each type of stiffness being measured, as shown in the graph in Fig. 4. The maximum applied load was slightly lower than the loads experienced during normal motorcycle operation. The graph also shows that as the load gradually increased, the clearence in the fixture were defined, affecting the overall stiffness values for both torsional and vertical

stiffness. At higher load values, the results became more precise, and the stiffness dependency on the load approached a constant value. Therefore, for the remainder of this work, we focus exclusively on the results from measurements with the maximum load.

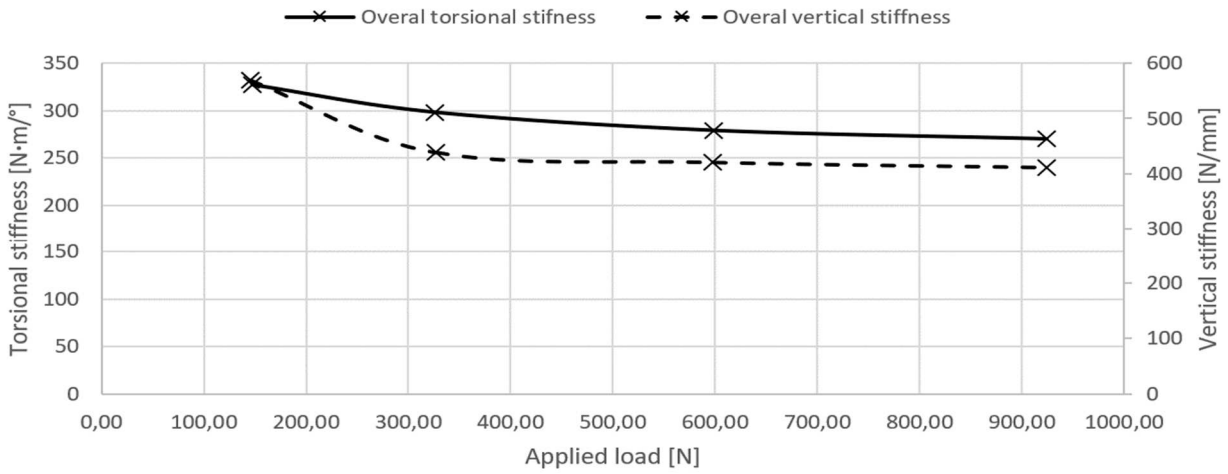

Fig. 4 *Measured stiffness to applied load graph*

3.1 Torsional stiffness

A simple fixture was designed to measure the torsional stiffness, as illustrated in Fig. 5, which generates a torsional moment acting on the swingarm. The part of the swingarm's connection to the frame was replaced with a rigid mount having zero degrees of freedom. The eccentric, which connects the swingarm to the wheel through the shaft, was replaced with bearings that allow one degree of freedom, the rotation. This replacement includes an arm with weights at its end, creating a torsional moment on the swingarm. The boundary conditions for the numerical simulation were chosen to match the experimental setup as closely as possible to ensure accurate comparison.

To evaluate the torsional stiffness, the relationship used is the ratio of the applied torsional moment to the resulting angle of twist.

$$K_T = \frac{M_K}{\alpha} \left[\frac{\mathrm{N \cdot m}}{^\circ}\right] \quad (1)$$

Where:
K_T…Torsional stiffness [N·m/°],
M_K…Torsional moment [N·m],
α…Twist angle [°].

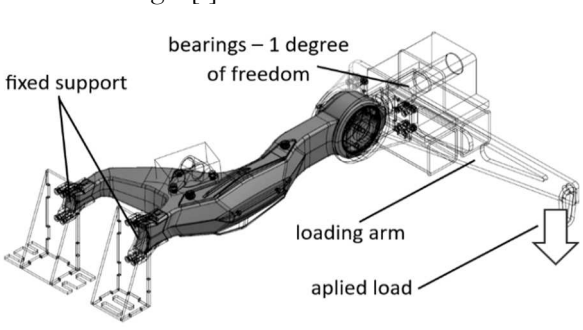

Fig. 5 *Torsional stiffness measuring fixture*

The torsional moment is determined by the length of the loading arm from the axis of twist and the applied force. The angle of twist for the overall torsional stiffness of the swingarm was evaluated based on the rotation of the plane defined by the reference points relative to the coordinate system in the axis of the torsional load. This is depicted in Fig. 6.

To evaluate the distribution of torsional stiffness along the length of the swingarm, a different method was necessary. This method involves calculating the angle of twist based on the displacement vector of a selected reference point due to deformation and its distance from the axis of twist. This approach is challenging given the complex, rotationally asymmetric geometry of the single-sided swingarm, which does not undergo pure torsion. This issue is illustrated in Fig. 7, where the normals of the displacement vectors (except for the dZ vector) of individual points in the cross-section do not intersect at a single point.

Since absolute precision is not crucial for this study, and the same issue is present in the simulation, a methodology was chosen that allows for a significantly easier calculation of the resulting angle of twist and the dependent torsional stiffness. Due to the pronounced plane of symmetry of the lower and upper halves of the swingarm, shown in Fig. 7 in the Y plane, it can be assumed that the axis of torsion passes through this plane. Therefore, the displacements of points along the Z-axis (dZ), parallel to the Y plane, and the distance of the investigated point from the plane of symmetry (Y) were evaluated at the investigated points. Subsequently, the angle of twist of the swingarm at a given point was calculated, converting from radians to degrees according to the relationship:

$$\propto = \tan\left|\frac{d_Z}{Y}\right| \cdot \frac{180}{\pi} \ [°] \qquad (2)$$

Where:

α…Twist angle [°],

d_Z…Point displacement in Z-axis [mm],

Y…Point Y coordinate from symmetry plane [mm].

The described procedure was applied to evaluate both the experimental measurements and the results of the FEA. The vector map at maximum torsional load, the coordinates, and the displacement of the selected points, as well as the overall angle of twist of the swingarm, are shown in Fig. 9.

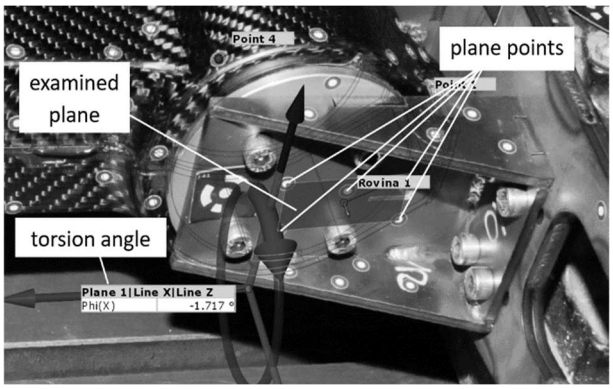

Fig. 6 *Detail of plane for twist angle derivation*

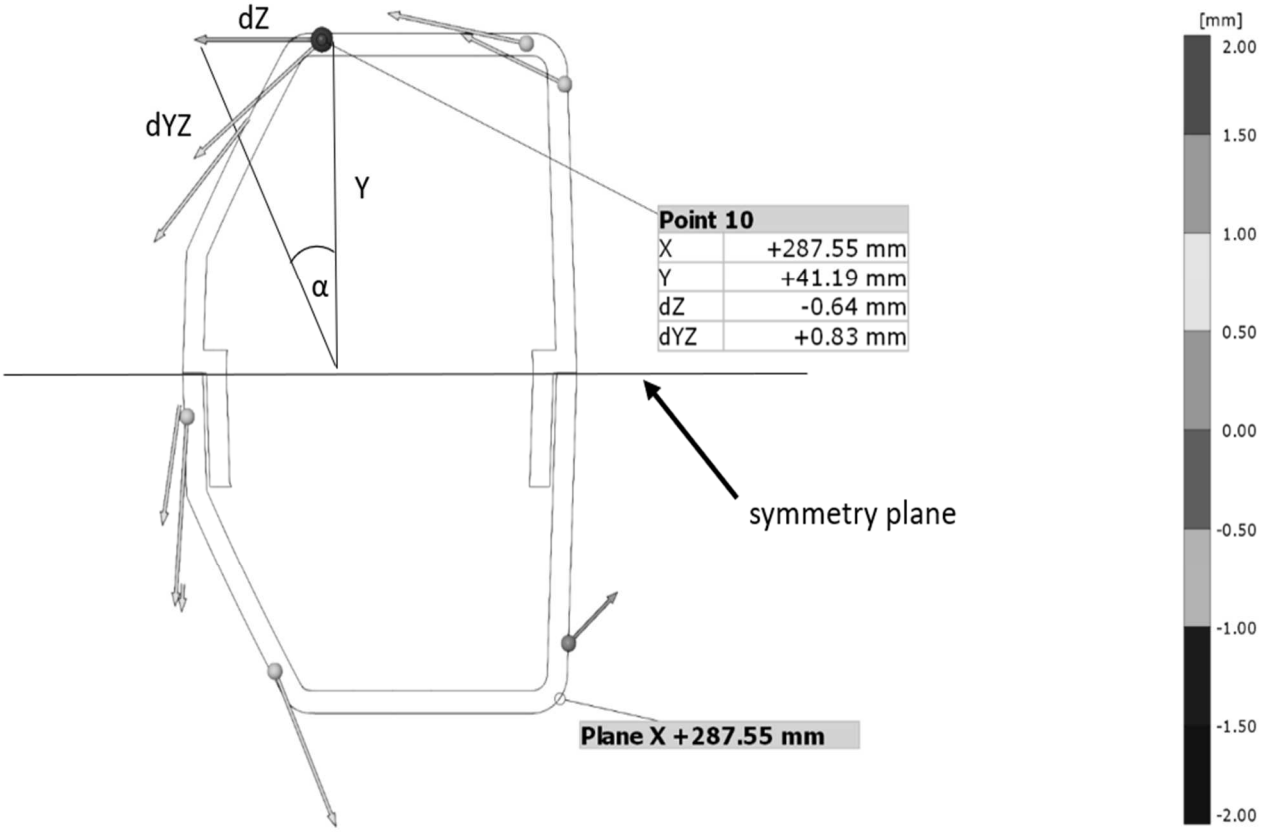

Fig. 7 *Twist angle calculation for point ten*

3.2 Vertical stiffness

For the vertical stiffness measurement, the fixture was slightly modified. The rigid mount with zero degrees of freedom remained in place at the connection of the swingarm to the frame. A significant change was the addition of a rigid substitution in place of the swingarm's suspension, which eliminated one degree of freedom in the vertical direction. The loading arm and bearing housings were removed from the part connecting the swingarm to the wheel. The weights were placed directly at the intersection of the wheel axis and the eccentric mount in the swingarm. The boundary conditions for the numerical simulation of vertical stiffness were chosen to match the mechanical measurements as closely as possible. The measuring setup is shown in Fig. 8.

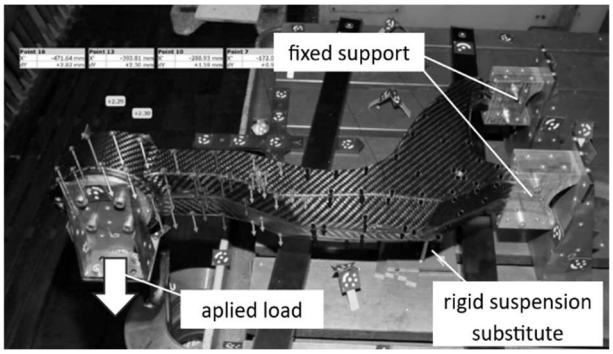

Fig. 8 *Vertical stiffness measuring setup*

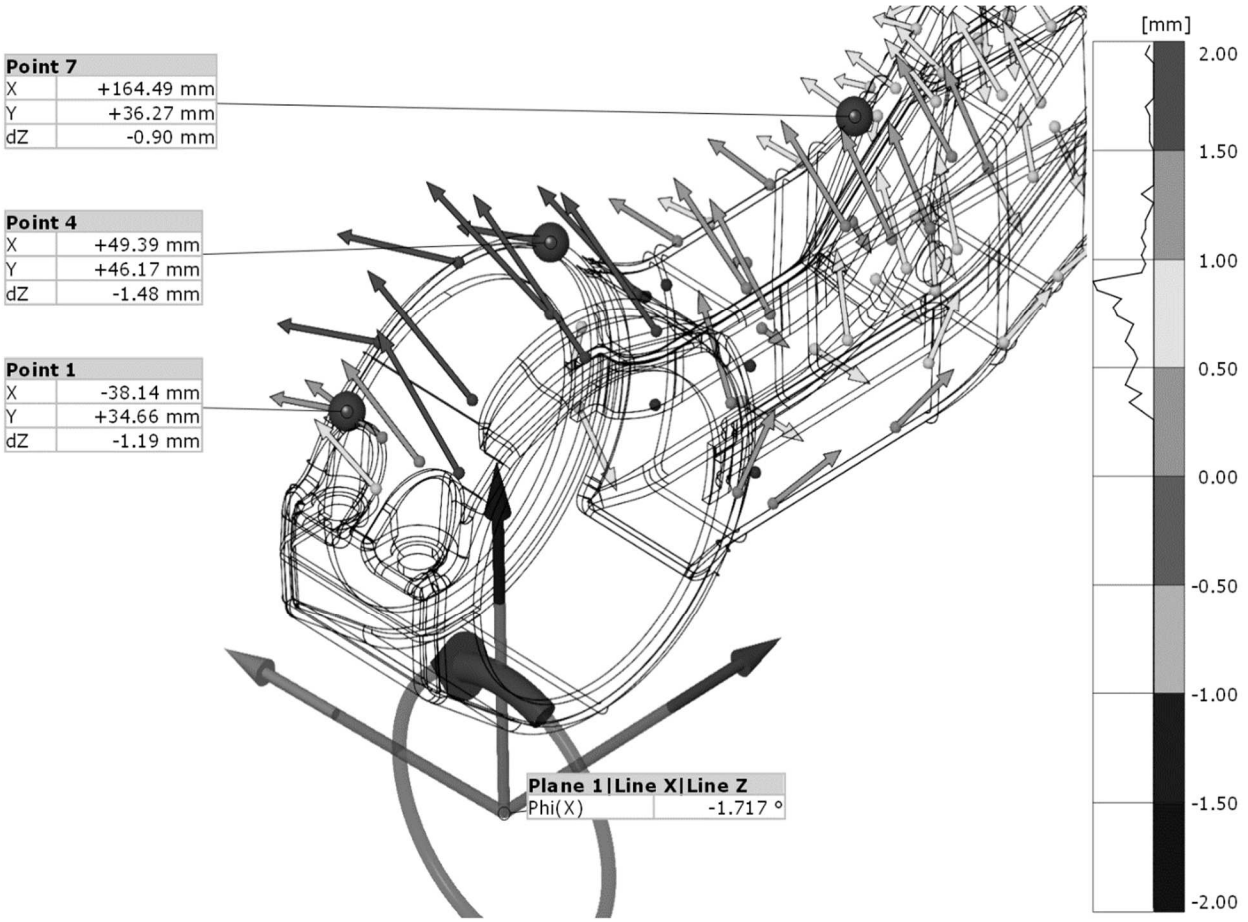

Fig. 9 *Deformation vectors at maximum torsion loading*

To evaluate vertical stiffness of the swingarm, the relationship used is the ratio of the applied vertical force to the resulting displacement of a point due to deformation.

$$K_v = \frac{F_V}{d_Y} \left[\frac{\mathrm{N}}{\mathrm{mm}}\right] \tag{3}$$

Where:

K_V…Vertical stiffness [N/mm],

F_V…Applied vertical load [N],

d_Y…Displacement in vertical direction [mm].

In contrast to the evaluation of the distribution of torsional stiffness, there are no complications for determining vertical stiffness. The process is straightforward, as it involves directly measuring the displacement resulting from a known vertical load.

4 Swingarm FE analysis

The resulting structural properties of the swingarm are significantly influenced by the part's layup, which is further affected by the material properties at the layer level. To increase the accuracy of the FEA of the swingarm, measurements of material properties were conducted. This approach was necessary because material constants can vary significantly depending on the type of fiber, manufacturer, weaving method, and processing techniques [6, 50, 51].

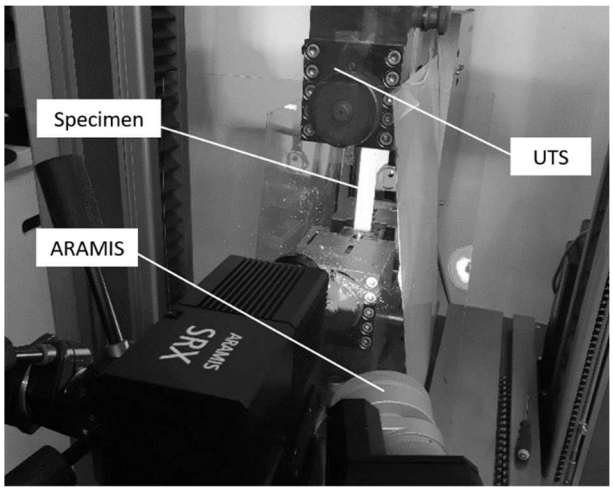

Fig. 10 *Material properties measuring setup*

The measurement and modification of the material model were conducted prior to the swingarm simulation. Unidirectional tension tests were performed according to ASTM D3039/D3039M [52] and ASTM E 132–97 [53] standards. Specimens were prepared according to the standarts, cut by waterjet and reinforced at the ends by glass fibre composite pads. Measurements and adjustments were made for Young's modulus, maximum tensile stress, maximum tensile strain, Poisson's ratio, and shear modulus. Other parameters

were obtained from relevant sources.

Testing was conducted on a universal testing machine (UTS) Zeiss Z100, which was synchronously connected to the optical measuring device GOM Aramis (Fig. 10). The evaluation was carried out using Digital Image Correlation (DIC), which allows for tracking the sample's deformation with subpixel accuracy using a stochastic pattern applied to the sample (Fig. 11). The resulting parameters used for the simulation are summarized in Tab. 4. [54–58].

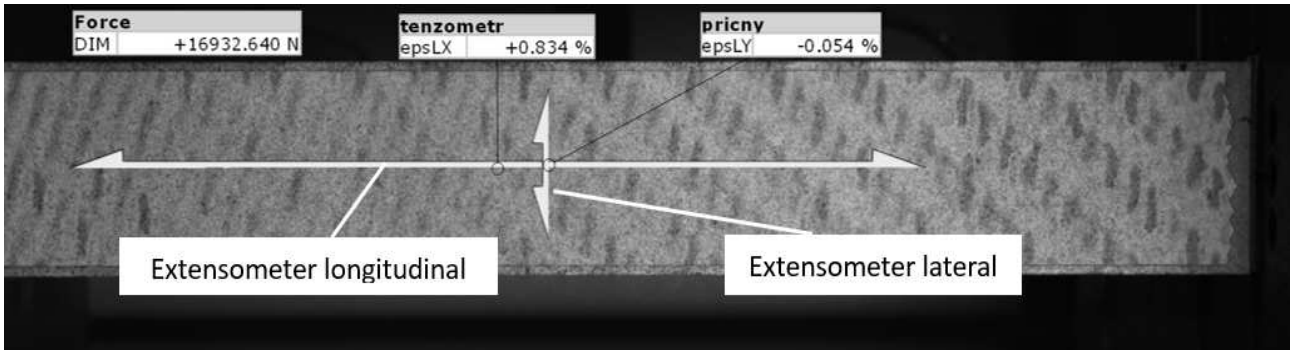

Fig. 11 *Aplied virtual extensometers - DIC*

Tab. 4 *Material model for FEA*

Material type	Wowen fabric	UD fabric
Orthotropic elasticity		
Young's modulus Ex [GPa]	67	134
Young's modulus Ey [GPa]	67	-
Poisson XY [-]	0.04	0.27
Poisson XZ [-]	-	0.27
Shear Modulus XY [GPa]	3.3	4.7
Shear Modulus XZ [GPa]	-	4.7
Orthotropic Stress Limits		
Tensile X [MPa]	1430	2860
Tensile Y [MPa]	1430	-
Shear XY [MPa]	125	60
Shear XZ [MPa]	-	60
Orthotropic strain limits		
Tensile X [-]	0.0202	0.0202
Tensile Y [-]	0.0202	-
Shear XY [-]	0.022	0.012
Shear XZ [-]	-	0.012

FEA simulations were conducted after the experimental measurements and were performed for both torsional and vertical stiffness. The boundary conditions and loads were set to match the conditions during the experimental measurements, ensuring comparability. The evaluation followed the same methods and relationships as described in the chapter 3 Experimental measuring. The only difference was that the simulation was conducted for a single load case: 462 N·m for torsional stiffness and 924 N for vertical stiffness.

The numerical simulation was conducted using Ansys Workbench. The elastic properties of the material obtained from tensile testing were assigned to the material model in the Engineering Data module. The biaxial fabric was set as two layers of perpendicular 150 g/m² UD fabric. Geometric simplifications were performed in Solidworks and SpaceClaim, and the mesh creation was done in Ansys Mechanical. The assignment of orthotropic properties to the shell and homogenization of the laminate were conducted in the ACP (Pre) module. The setting of boundary conditions, loading, and evaluation were performed in the Ansys Mechanical module, with further evaluation also conducted in ACP (Post). The solver used for the simulation was Ansys Mechanical APDL.

For simulating composite components, shell geometry was used, while volumetric geometry was used for aluminum inserts. Bonded joints in the simulation were replaced with a rigid bonded constraint. The discretization of composite parts utilized the 4-node shell element, Shell 181. The element size was nominally set to 2.2 mm, providing sufficient accuracy and rapid computation. The mesh density is shown in Fig. 12. The boundary conditions of the simulation were adapted to closely match the actual fixture and loading conditions during measurement.

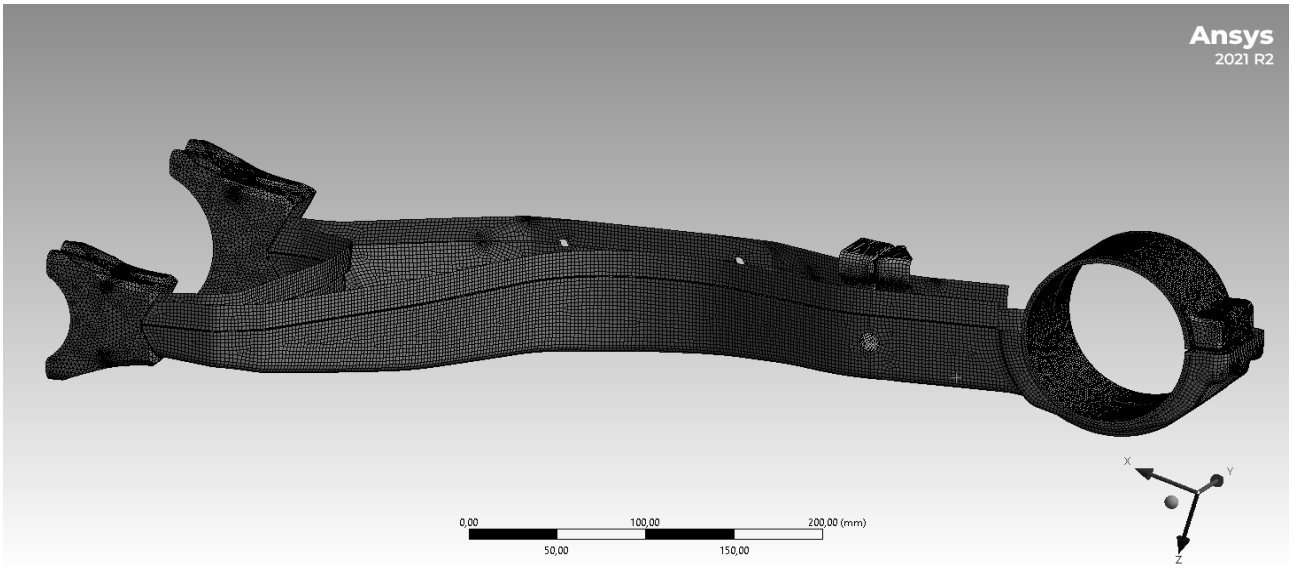

Fig. 12 *Mesh density*

5 Results and discussion

5.1 Torsional stiffness results

During the simulation with a torsional load of 462 N·m, the twist angle was 1.85°, resulting in an overall torsional stiffness of 249 N·m/° for the swingarm. In the experimental measurement under the same load, the twist angle was 1.72°, with an overall stiffness of 270 N·m/°. This represents a difference of 7.7% in favor of the experimental measurement. Compared to the literature (Tab. 1), this is a low stiffness value within the range of measured swingarms but does not meet the range specified by Cossalter [5].

The distribution of stiffness from the simulation and experimental measurement is shown in Fig. 13. The figure highlights a correlation between the simulated and measured results, though the variability in some areas reaches up to 200 N·m/°. This discrepancy could be attributed to the methodology used and the low displacement values of points near the fixed mount of the swingarm.

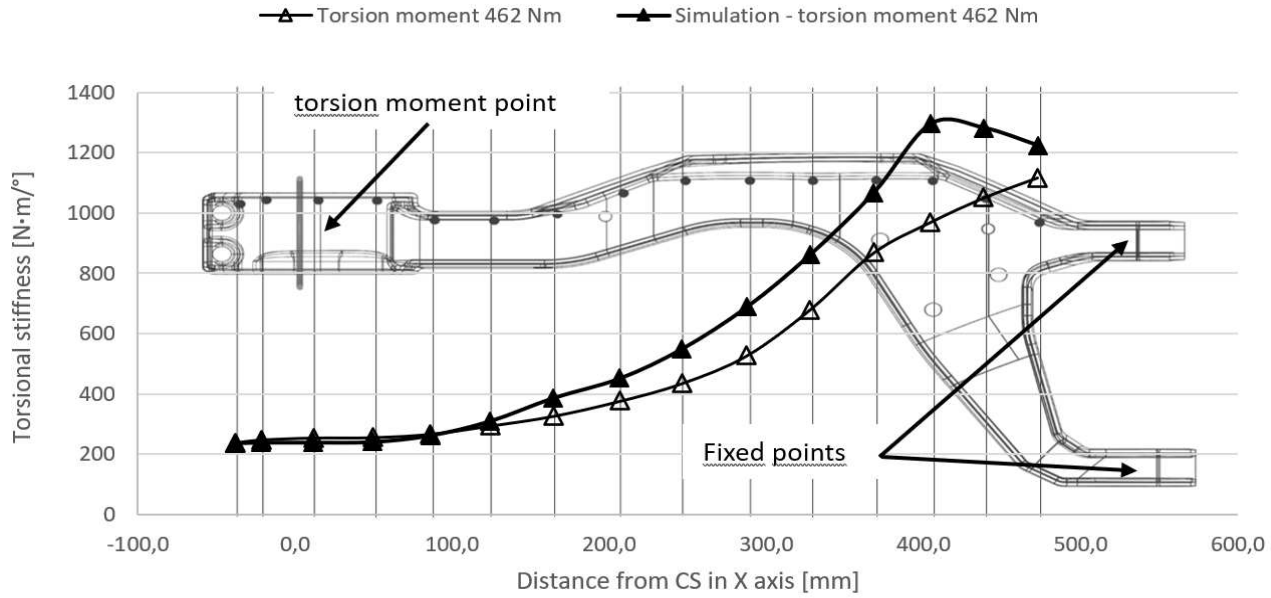

Fig. 13 *Torsional stiffness distribution*

5.2 Vertical stiffness results

During the simulation with an applied force of 924 N for the vertical stiffness of the swingarm, the overall value was found to be 414 N/mm, while real testing yielded a value of 411 N/mm. This represents a difference of 0,7% in favor of the simulation. Compared to values reported in the literature (Tab. 1), these values are lower, primarily due to the geometry of the

swingarm, which has a relatively low second moment of area, and the test layup, which is significantly more economical compared to, for example, Airoldi's work [38]. Nevertheless, the value should be sufficient to meet the requirement of having stiffness at least five times higher than the spring stiffness (50 N/mm).

Examining the distribution of stiffness in Figure (Fig. 14), one can observe a correlation between the simulated and measured stiffness. However, in some areas, the values differ by up to 200 N/mm. This discrepancy is due to differences between reality and the simplified simulation model. Therefore, it can be concluded that the small overall stiffness difference between the simulation and the measurement for such a complex structure is likely coincidental.

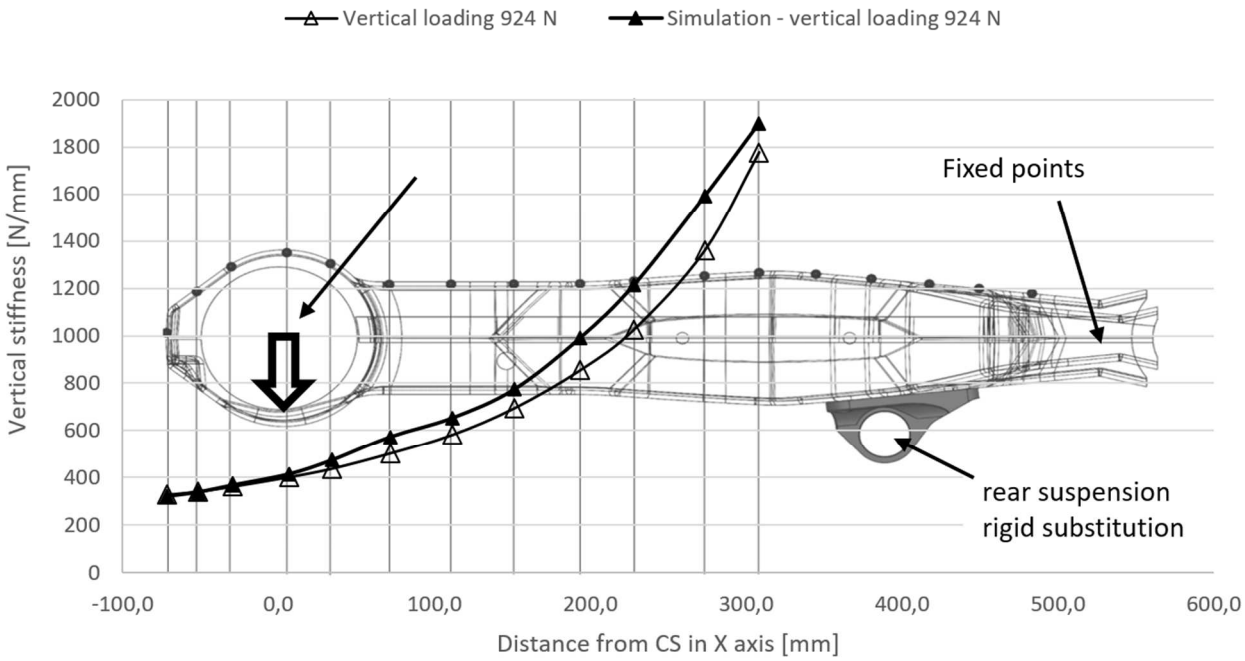

Fig. 14 *Vertical stiffness distribution*

6 Conclusions

- Measuring the structural characteristics of the swingarm using photogrammetry is an efficient method that enables quantification under static load conditions. Compared to conventional methods, it allows parallel tracking of deformation on a cloud of reference points and the possibility of additional analyses even after the measurement is complete. This enables verification of FEA results not only for overall stiffness but also along the length of the swingarm. This approach provides useful information and allows the evaluation of critical areas with the highest gradient of stiffness reduction.

Tab. 5 *Overall structural stiffness results*

	Torsional characteristics [N·m/°]	**Vertical characteristics [N/mm]**
Overall stiffness - simulation	249	414
Overall stiffness - measuring	270	411
Difference	7.7 %	-0.7 %

- The presented results show significant discrepancies between simulation and measurement. The overall difference between numerical simulation and experimental measurement is 7.7% for torsional stiffness and -0.7% for vertical stiffness. These differences are mainly due to the complex geometry, the sensitivity of manufacturing technology to precision, simplified geometry for computational ease, and methodological limits, particularly for torsional stiffness. However, these

differences can be considered acceptable and representative.

- In terms of torsional stiffness, the values did not meet the reference values according to Cossalter [5], indicating substantial room for modification. Nonetheless, the current value exceeds those reported by other authors, suggesting that the swingarm should function adequately (Tab. 1).
- For vertical stiffness, the condition of significantly higher stiffness was met, ensuring the proper function of the motorcycle's suspension, although there is still room for improvement. One primary reason for the lower stiffness is the simple design of the swingarm, which has a low second moment of area compared to other swingarms in Tab. 1.
- The manufactured swingarm had a simple layup without any optimization, with the primary goal of concept verification and numerical simulation validation. Based on the findings of this study, it is possible to optimize the layup to increase stiffness under the required loads by adding additional layers, local reinforcements, or using high-modulus fibers, potentially through multi-objective optimization.
- Objective goals for swingarm design optimization should be maximize torsional stiffness (1000 – 2000 N·m/°), maximize vertical stiffness (500 – 1500 N/mm), reduce lateral stiffness (800 – 1600 N/mm), minimize weight and ensure sufficient strength and safety for worst case scenarios (Tab. 2).

Acknowledgement

This research study was supported by the grant "Modern Technologies for the Processing of Advanced Materials Used for Interdisciplinary Applications", FSI-S-22-7957.

References

[1] LAKE, K., THOMAS, R., WILLIAMS, O. (2012). The influence of compliant chassis components on motorcycle dynamics: an historical overview and the potential future impact of carbon fibre. In: *Vehicle System Dynamics*, Vol. 50, No. 7, pp. 1043–1052. ISSN 0042-3114. From: doi:10.1080/00423114.2011.647824

[2] SHARP, R. S. (1971). The Stability and Control of Motorcycles. In: *Journal of Mechanical Engineering Science*, Vol. 13, No. 5, pp. 316–329. ISSN 0022-2542. From: doi:10.1243/JMES_JOUR_1971_013_051_02

[3] COSSALTER, V., DALLA, G., LOT, R., MASSARO, M. (2009). An advanced multibody model for the analysis of motorcycle dynamics. R. China.

[4] SCHIEHLEN, W. (1990). *Multibody Systems Handbook*. 1st ed. Springer Berlin Heidelberg, Berlin, Heidelberg. ISBN 978-3-642-50997-1. From: doi:10.1007/978-3-642-50995-7

[5] COSSALTER, V. (2006). *Motorcycle dynamics*. 2nd English ed. Lulu. ISBN 978-1-4303-0861-4.

[6] KULÍŠEK, V. (2021). Výpočty kompozitních komponent pomocí metody konečných prvků. In: Praha. 5. červenec 2021.

[7] EVANGELOU, S., LIMEBEER, D. J. N., SHARP, R. S., SMITH, M. C. (2006). An H-Loop-Shaping Approach to Steering Control for High-Performance Motorcycles. In: *Control of Uncertain Systems: Modelling, Approximation, and Design*, pp. 257–275. Springer-Verlag, Berlin/Heidelberg. From: doi:10.1007/11664550_14

[8] SHARP, R. S., ALSTEAD, C. J. (1980). The Influence of Structural Flexibilities on the Straight-running Stability of Motorcycles. In: *Vehicle System Dynamics*, Vol. 9, No. 6, pp. 327–357. ISSN 0042-3114. From: doi:10.1080/00423118008968629

[9] SPLERINGS, P. T. J. (1981). The Effects of Lateral Front Fork Flexibility on the Vibrational Modes of Straight-Running Single-Track Vehicles. In: *Vehicle System Dynamics*, Vol. 10, No. 1, pp. 21–35. ISSN 0042-3114. From: doi:10.1080/00423118108968633

[10] LIMEBEER, D. J. N., SHARP, R. S. (2006). Bicycles, motorcycles, and models. In: *IEEE Control Systems*, Vol. 26, No. 5, pp. 34–61. ISSN 1066-033X. From: doi:10.1109/MCS.2006.1700044

[11] KANE, T. R. (1978). The Effect of Frame Flexibility on High Speed Weave of Motorcycles. From: doi:10.4271/780306

[12] SHARP, R. S., EVANGELOU, S., LIMEBEER, D. J. N. (2004). Advances in the Modelling of Motorcycle Dynamics. In: *Multibody System Dynamics*, Vol. 12, No. 3, pp. 251–

283. ISSN 1384-5640. From: doi:10.1023/B.0000049195.60868.a2

[13] VERMA, M. K., SCOTT, R. A., SEGEL, L. (1980). Effect of Frame Compliance on the Lateral Dynamics of Motorcycles. In: *Vehicle System Dynamics*, Vol. 9, No. 4, pp. 181–206. ISSN 0042-3114. From: doi:10.1080/00423118008968622

[14] ROE, G. E., THORPE, T. E. (1989). The Influence of Frame Structure on the Dynamics of Motorcycle Stability. From: doi:10.4271/891772

[15] COSSALTER, V., LOT, R., MASSARO, M. (2007). The influence of frame compliance and rider mobility on the scooter stability. In: *Vehicle System Dynamics*, Vol. 45, No. 4, pp. 313–326. ISSN 0042-3114. From: doi:10.1080/00423110600976100

[16] LOT, R., COSSALTER, V., MASSARO, M. (2005). The significance of frame compliance and rider mobility on the motorcycle stability. In: *Multibody dynamics*.

[17] SHARP, R. S. (1974). The Influence of Frame Flexibility on the Lateral Stability of Motorcycles. In: *Journal of Mechanical Engineering Science*, Vol. 16, No. 2, pp. 117–120. ISSN 0022-2542. From: doi:10.1243/JMES_JOUR_1974_016_021_02

[18] FOALE, T. (2002). Motorcycle handling and chassis design: the art and the science.

[19] SMITH, B., KIENHOFER, F. (2014). Development of a carbon fibre swingarm. In: *9th South African Conference on Computational and Applied Mechanics*, SACAM 2014.

[20] THEDE, P., PARKS, L. (2010). *Race Tech's Motorcycle Suspension Bible*. Quarto Publishing Group USA. ISBN 1610591666.

[21] TARABORRELLI, L., FAVARON, V., DORIA, A. (2017). The effect of swingarm stiffness on motorcycle stability: experimental measurements and numerical simulations. In: *International Journal of Vehicle Systems Modelling and Testing*, Vol. 12, No. 3–4, pp. 240–261. ISSN 1745-6436. From: doi:10.1504/IJVSMT.2017.089981

[22] ARMENTANI, E., FUSCO, S., PIROZZI, M. (2007). Numerical evaluation and experimental tests for a road bike swingarm. In: *Science and Motor Vehicles JUMV International Automotive Conference with Exhibition*.

[23] RISITANO, G., SCAPPATICCI, L., GRIMALDI, C., MARIANI, F. (2012). Analysis of the Structural Behavior of Racing Motorcycle Swingarms. From: doi:10.4271/2012-01-0207

[24] FEARNEY, P. (2020). The man who pioneered carbon fibre F1 cars: still saving lives today. In: *Motor Sport Magazine*.

[25] PURVIS, B. (2014). Carbon-fibre bikes - a potted history. In: *Motorcycle News*.

[26] CAPSONI, D., BINI, M., FERRARI, S., MUSTARELLI, P. (2015). Lithium-Air Batteries Based on Carbon Nanomaterials. In: *Carbon Nanomaterials for Advanced Energy Systems*, pp. 385–405. John Wiley & Sons, Inc, Hoboken, NJ. From: doi:10.1002/9781118980989.ch12

[27] NAQVI, A. A., ZAHOOR, A., SHAIKH, A. A., BUTT, F. A., RAZA, F., AHAD, I. U. (2022). Aprotic lithium air batteries with oxygen-selective membranes. In: *Materials for Renewable and Sustainable Energy*, Vol. 11, No. 1, pp. 33–46. ISSN 2194-1459. From z: doi:10.1007/s40243-021-00205-w

[28] ZHU, K., WANG, C., CHI, Z., KE, F., YANG, Y., WANG, A., WANG, W., MIAO, L. (2019). How Far Away Are Lithium-Sulfur Batteries From Commercialization? In: *Frontiers in Energy Research*, Vol. 7. ISSN 2296-598X. From: doi:10.3389/fenrg.2019.00123

[29] NOVUS. (2023). Novus bike. Novus GmbH. From: https://novusbike.com/bike-2/

[30] Samurai bike. (2024). From: https://www.denzel.bike/samurai/

[31] JEC Observer (2023). Overview of the global composites market 2022-2027.

[32] JEC Observer (2023). PRESS KIT 2 JEC Observer • PRESS KIT •.

[33] ZOUHAR, J., SLANÝ, M., SEDLÁK, J., JOSKA, Z., POKORNÝ, Z., BARÉNYI, I., MAJERÍK, J., FIALA, Z. (2022). Application of Carbon–Flax Hybrid Composite in High Performance Electric Personal Watercraft. In: *Polymers*, Vol. 14, No. 9, p. 1765. ISSN 2073-4360. From: doi:10.3390/polym14091765

[34] KUPČÁK, R., ZOUHAR, J. (2020). Application of composite materials in sports optics. In: *Manufacturing Technology*, Vol. 20, No. 2, pp. 200–209. ISSN 12132489. From: doi:10.21062/mft.2020.038

[35] VILIŠ, J., POKORNÝ, Z., ZOUHAR, J., JOPEK, M. (2022). Ballistic Resistance of

Composite Materials Tested by Taylor Anvil Test. In: *Manufacturing Technology*, Vol. 22, No. 5, pp. 610–616. ISSN 12132489. From: doi:10.21062/mft.2022.074

[36] ODOM, E. M. (1982). Design and fabrication of a motorcycle swingarm utilizing composite materials. United States -- Wyoming. From: https://www.proquest.com/dissertations-theses/design-fabrication-motorcycle-swingarm-utilizing/docview/303245778/se-2?accountid=17115

[37] TAFAGHODI HELALI, H., GRAFINGER, M. (2016). The precision of FEM simulation results compared with theoretical composite layup calculation. In: *Composites Part B: Engineering*, Vol. 95, pp. 282–292. ISSN 13598368. From: doi:10.1016/j.compositesb.2016.04.003

[38] AIROLDI, A., BERTOLI, S., LANZI, L., SIRNA, M., SALA, G. (2012). Design of a Motorcycle Composite Swing-Arm by Means of Multi-objective Optimisation. In: *Applied Composite Materials*, Vol. 19, No. 3–4, pp. 599–618. ISSN 0929-189X. From: doi:10.1007/s10443-011-9227-6

[39] RAO, H. M., KANG, J., HUFF, G., AVERY, K., SU, X. (2017). Impact of Rivet Head Height on the Tensile and Fatigue Properties of Lap Shear Self-Pierced Riveted CFRP to Aluminum. In: *SAE International Journal of Materials and Manufacturing*, Vol. 10, No. 2, pp. 2017-01–0477. ISSN 1946-3987. From: doi:10.4271/2017-01-0477

[40] LI, L. (2004). Failure analysis of aluminum alloy swing arm welded joints. In: *Journal of Failure Analysis and Prevention,* Vol. 4, No. 3, pp. 52–57. ISSN 1547-7029. From: doi:10.1007/s11668-996-0015-9

[41] SWOLFS, Y., VERPOEST, I., GORBATIKH, L. (2019). Recent advances in fibre-hybrid composites: materials selection, opportunities and applications. In*: International Materials Reviews*, Vol. 64, No. 4, pp. 181–215. ISSN 0950-6608. From: doi:10.1080/09506608.2018.1467365

[42] HARRIS, C. E., STARNES, J. H., SHUART, M. J. (2002). Design and Manufacturing of Aerospace Composite Structures, State-of-the-Art Assessment. In: *Journal of Aircraft*, Vol. 39, No. 4, pp. 545–560. ISSN 0021-8669. From: doi:10.2514/2.2992

[43] GUPTA, M. K., SRIVASTAVA, R. K. (2016). Mechanical Properties of Hybrid Fibers-Reinforced Polymer Composite: A Review. In: *Polymer-Plastics Technology and Engineering*, Vol. 55, No. 6, pp. 626–642. ISSN 0360-2559. From: doi:10.1080/03602559.2015.1098694

[44] ZHANG, W., XU, J. (2022). Advanced lightweight materials for Automobiles: A review. In: *Materials & Design*, Vol. 221, p. 110994. ISSN 02641275. From: doi:10.1016/j.matdes.2022.110994

[45] ZHU, L., LI, N., CHILDS, P. R. N. (2018). Light-weighting in aerospace component and system design. In: *Propulsion and Power Research*, Vol. 7, No. 2, pp. 103–119. ISSN 2212540X. From: doi:10.1016/j.jppr.2018.04.001

[46] KUPČÁK, R., ZOUHAR, J., VILIŠ, J., GREGOR, L., HRUŠECKÁ, D. (2023). Precision and Dimensional Stability of Bonded Joints of Carbon-Fibre-Reinforced Polymers Parts. In: *Applied Sciences*, Vol. 13, No. 18, p. 10413. ISSN 2076-3417. From: doi:10.3390/app131810413

[47] ABRAHAM, D., MATTHEWS, S., MCILHAGGER, R. (1998). A comparison of physical properties of glass fibre epoxy composites produced by wet lay-up with autoclave consolidation and resin transfer moulding. In: *Composites Part A: Applied Science and Manufacturing*, Vol. 29, No. 7, pp. 795–801. ISSN 1359835X. From: doi:10.1016/S1359-835X(98)00055-4

[48] BAQERSAD, J., POOZESH, P., NIEZRECKI, C., AVITABILE, P. (2017). Photogrammetry and optical methods in structural dynamics – A review. In: *Mechanical Systems and Signal Processing*, Vol. 86, pp. 17–34. ISSN 08883270. From: doi:10.1016/j.ymssp.2016.02.011

[49] LIU, T., BURNER, A. W., JONES, T. W., BARROWS, D. A. (2012). Photogrammetric techniques for aerospace applications. In: *Progress in Aerospace Sciences*, Vol. 54, pp. 1–58. ISSN 03760421. From: doi:10.1016/j.paerosci.2012.03.002

[50] JONES, R. M. (2018). *Mechanics of Composite Materials*. CRC Press. ISBN 9781315272986. From: doi:10.1201/9781498711067

[51] JURAČKA, J. Kompozitní konstrukce v letectví.

[52] ASTM INTERNATIONAL. (2002). D 3039/D 3039M - 00.

[53] ASTM INTERNATIONAL. (2017). E 132 - 97 Standart test method for poisson's ratio at room temperature.

[54] TEKIELI, M., DE SANTIS, S., DE FELICE, G., KWIECIEŃ, A., ROSCINI, F. (2017). Application of Digital Image Correlation to composite reinforcements testing. In: *Composite Structures*, Vol. 160, pp. 670–688. ISSN 02638223. From: doi:10.1016/j.compstruct.2016.10.096

[55] HLIVA, V., SZEBÉNYI, G. (2023). Non-Destructive Evaluation and Damage Determination of Fiber-Reinforced Composites by Digital Image Correlation. In*: Journal of Nondestructive Evaluation*, Vol. 42, No. 2. ISSN 15734862. From: doi:10.1007/s10921-023-00957-7

[56] HOLMES, J., SOMMACAL, S., DAS, R., STACHURSKI, Z., COMPSTON, P. (2023). Digital image and volume correlation for deformation and damage characterisation of fibre-reinforced composites: A review. In: *Composite Structures*, Vol. 315, p. 116994. ISSN 0263-8223. From: doi:https://doi.org/10.1016/j.compstruct.2023.116994

[57] BOGUSZ, P. (2023). Digital Image Correlation Analysis of Strain Fields in Fibre-Reinforced Polymer–Matrix Composite under ±45° Off-Axis Tensile Testing. In: *Polymers*, Vol. 15, No. 13. ISSN 20734360. From: doi:10.3390/polym15132846

[58] DUFOUR, J. E., COLANTONIO, G., BOUVET, C., PÉRIÉ, J. N., PASSIEUX, J. C., SERRA, J. (2023). Monitoring structural scale composite specimens in a post-buckling regime: The integrated finite element stereo digital image correlation approach with geometrically non-linear regularization Monitoring structural scale composite specimens in post-buckling regime: the Integrated Finite-Element Stereo Digital Image Correlation approach with geometrically non-linear regularization. From: doi:10.1111/str.12450